



Metal phthalocyanine-based conjugated microporous polymer/carbon nanotube composites as flexible electrodes for supercapacitors

Lan Mei^a, Xu Cui^a, Juncheng Wei^a, Qian Duan^{a,b,*}, Yanhui Li^a

^a School of Materials Science and Engineering, Changchun University of Science and Technology, Changchun, 130022, China

^b Engineering Research Center of Optoelectronic Functional Materials, Ministry of Education, Changchun, 130022, China

ARTICLE INFO

Keywords:

Metal phthalocyanine
Conjugated microporous polymer
Carbon nanotubes
Supercapacitors
Flexible electrode

ABSTRACT

Conjugated microporous polymers with active functional groups have attracted more and more attentions in energy conversion systems. However, their low electrical conductivity results in low capacitance, thus limiting their practical application. Herein, conjugated microporous polymer with triphenylamine aldehyde linked to metal phthalocyanines (MNC) is synthesized and then compounded with high-conductivity carbon nanotubes (CNTs) (denoted as CoNCCs) by vacuum filtration. Moreover, CoNCCs exhibit flexibility, which could be served as a self-standing and binder-free flexible electrode of supercapacitors. As a result, the optimized CoNCCs as the flexible electrode show high specific capacitance of 213.4 F g^{-1} at 0.5 A g^{-1} . In addition, the higher capacity retention rate 85.3% can be retained after 1750 cycles at 20 A g^{-1} . The good electrochemical properties can be attributed to the synergistic effect and strong dual-phase interaction between MNC and CNTs. This work opens the way to develop high-performance and low environmental footprint organic electrode materials for SCs.

1. Introduction

The energy crises and consumption of resources concerning the environment have aroused our crisis consciousness and requirement for the development of effective and renewable energy storage technology [1–3]. Electrochemical energy storage equipment has played an extremely important role in solving energy shortages [4]. Supercapacitors (SCs) with high rate performance, excellent cycle stability, high power density and environment-friendly properties are considered as promising energy storage devices [5–7]. SCs include two categories: pseudocapacitors and electrochemical double-layer capacitors (EDLCs). Considering that the working mechanisms, the pseudocapacitors store electrical energy through the reversible redox reaction of electrode materials. By contrast, the EDLCs store electrical energy through rapid and reversible adsorption and desorption of the electrolytic ions at the electrode/electrolyte interface [8,9]. No matter which type of SCs, the influence of the electrode materials on its electrochemical performance is crucial [10,11]. In recent years, inorganic electrode materials have been extensively widely used in SCs, but most of them have a few defects, for instance the resource shortage and environmental contamination during the mining process. Thus, efforts have been made to develop cheaper and more environment-friendly electrode materials to

solve this problem [12,13].

Organic electrode materials have aroused widespread attentions in view of their advantages of environmental friendliness, low energy consumption and high redox activity [14–16]. As a type of important organic electrode material, conjugated microporous polymers (CMPs) have been widely used in SCs due to their abundant pore structure and structural tenability [17–19]. Generally, CMPs are composed of some specific structure unit and linking group, in which the specific structure unit with redox activity could endow them with high electrochemical performance. In this context, phthalocyanines peculiarly metallophthalocyanines (MPcs), a type of 18-electron coplanar aromatic macrocycles could be used as the vital functional π -conjugated structural units [20–22]. MPcs and their derivant are known to be excellent organic semiconductors with potential applications in many fields [23–26]. Thus, CMPs based on MPcs are considered as a type of fascinating electrode materials for energy conversion systems [27–30]. Whereas, the inherent low electrical conductivity of CMPs results in low capacitance. To improve the conductivity of CMPs, combining low-conductivity CMPs with high-conductivity carbon materials, including graphene and carbon nanotubes (CNTs), is an effective strategy [31–33]. Among them, CNTs have aroused great scientific attention in view of their unique flexible, mechanical, electronic and structural

* Corresponding author. School of Materials Science and Engineering, Changchun University of Science and Technology, Changchun, 130022, China.
E-mail address: duanqian88@hotmail.com (Q. Duan).

properties. Some studies have shown that the introduction of CNTs can improve the activity resulted from the large surface area and excellent electronic properties [34–36]. Therefore, it is important to construct flexible and integrated electrode based on CMPs and CNTs for SCs.

Herein, we prepared the composite film composed of CMP with triphenylamine aldehyde linked to metal phthalocyanines ($M = \text{Co}$ and Fe) and high-conductivity CNTs by using the microwave method as well as the vacuum filtration strategy, which are the binder-free and free-standing flexible electrode of SCs. Profiting by the strong π - π interaction and synergistic effect between MNC and CNTs, the optimized CoNCCs show high specific capacitance of 213.4 F g^{-1} at 0.5 A g^{-1} and good capacity retention of 85.3% after 1750 cycles at 20 A g^{-1} . This work opens up the way to construct high-performance flexible SCs by reasonable recombination of MNC with highly conductive CNTs.

2. Experimental details

2.1. Synthesis of samples

2.1.1. Synthesis of tetra-nitro metallophthalocyanine ($\text{MPc}(\text{NO}_2)_4$, $M = \text{Co}, \text{Fe}$)

Typically, the tetra-nitro metallophthalocyanine ($\text{MPc}(\text{NO}_2)_4$) was synthesized by solid phase reaction [37], which was reacted with 4-nitrophthalonitrile (3.8 g, 0.02 mol), $\text{CoCl}_2 \cdot 6\text{H}_2\text{O}$ (1.2 g, 0.005 mol), urea (9.6 g, 0.16 mol) and an appropriate amount of ammonium molybdate in a 250 mL round bottom flask at 160°C under reflux for 5 h. Then, the product was stirred magnetically with hydrochloric acid (HCl) solution (0.2 L , 1 mol L^{-1}) and sodium hydroxide (NaOH) solution (0.2 L , 1 mol L^{-1}) at 90°C for 1 h. Finally, the product was filtered and washed repeatedly with deionized water to neutral and then dried in a vacuum drying oven to give a dark green solid in 78% isolated yield. IR (KBr, cm^{-1}): 1521, 1339, 1140, 1093, 846, 760, 726; MALDI-TOF-MS m/z : calc. for $\text{C}_{32}\text{H}_{12}\text{N}_{12}\text{O}_8\text{Co}$ [$M\text{-H}$] $^+$: 751.0; found 751.2; Anal. calcd (%) for $\text{C}_{32}\text{H}_{12}\text{N}_{12}\text{O}_8\text{Co}$: C, 51.15; H, 1.61; N, 22.37; O, 17.03. Found: C, 51.47; H, 1.52; N, 22.62; O, 16.87.

2.1.2. Synthesis of tetra-amino metallophthalocyanines ($\text{MPc}(\text{NH}_2)_4$, $M = \text{Co}, \text{Fe}$)

The cobalt tetra-amino-phthalocyanines ($\text{CoPc}(\text{NH}_2)_4$) was synthesized from $\text{CoPc}(\text{NO}_2)_4$ [38,39]. Concretely, the $\text{CoPc}(\text{NO}_2)_4$ (1.5 g, 0.002 mol) and $\text{Na}_2\text{S} \cdot 9\text{H}_2\text{O}$ (5.8 g, 0.074 mol) were dissolved in *N,N*-dimethylformamide (DMF, 30 mL) and then reacted at 60°C for 1 h. Subsequently, the deionized water (500 mL) was added into the above solution and the cyan $\text{CoPc}(\text{NH}_2)_4$ was obtained by centrifugation and washed with water to neutral and then dried under vacuum. The $\text{FePc}(\text{NH}_2)_4$ was synthesized by the same procedure only replacing $\text{CoCl}_2 \cdot 6\text{H}_2\text{O}$ using $\text{FeCl}_2 \cdot 4\text{H}_2\text{O}$. The isolated yields of the $\text{CoPc}(\text{NH}_2)_4$ and $\text{FePc}(\text{NH}_2)_4$ were 56% and 72%, respectively. IR (KBr, cm^{-1}): 3344, 3221, 1609, 1496, 1345, 1092, 830, 747, 655; MALDI-TOF-MS m/z : calc. for $\text{C}_{32}\text{H}_{20}\text{N}_{12}\text{Co}$ [$M\text{-H}$] $^+$: 631.1; found 631.3; Anal. calcd (%) for $\text{C}_{32}\text{H}_{20}\text{N}_{12}\text{Co}$: C, 60.86; H, 3.19; N, 26.62. Found: C, 61.15; H, 3.32; N, 26.34.

2.1.3. Synthesis of 4',4'',4'''-nitrotris([(1,1'-biphenyl)-4-carbaldehyde]) (NBC)

Tris(4-iodophenyl)amine (0.16 mmol) and 4-formylphenylboronic acid (0.48 mmol) were dissolved in 10 mL of tetrahydrofuran (THF) [40,41] and then K_2CO_3 aqueous solution (5.0 mL, 2.0 mol L^{-1}) and bis(triphenylphosphine)palladium(II) dichloride (30 mg) was added in sequence under nitrogen atmosphere. After the mixture was refluxed for 12 h, the obtained solution was extracted twice with dichloromethane ($3 \times 100 \text{ mL}$). The residue was chromatographed on a silica gel column to get yellow solid with 72% yield. $^1\text{H NMR}$ (400 MHz, CDCl_3): δ (ppm) 10.05 (s, 3H, -CHO), 7.96 (d, $J = 8.0 \text{ Hz}$, 6H, Ar-H), 7.77 (d, $J = 8.0 \text{ Hz}$, 6H, Ar-H), 7.62 (d, $J = 8.0 \text{ Hz}$, 6H, Ar-H), 7.29 (d, $J = 8.0 \text{ Hz}$, 6H, Ar-H); IR (KBr, cm^{-1}): 3032, 2830, 2732, 1701, 1590, 1525, 1499,

1285, 1180, 824, 714, 649, 571; Anal. calcd (%) for $\text{C}_{39}\text{H}_{27}\text{NO}_3$: C, 84.00; H, 4.88; N, 2.51; O, 8.61. Found: C, 83.85; H, 4.96; N, 2.44; O, 8.78.

2.1.4. Synthesis of MNC ($M = \text{Co}, \text{Fe}$)

Specifically, $\text{CoPc}(\text{NH}_2)_4$ (0.06 mmol, 30 mg) and NBC (0.08 mmol, 45 mg) were dissolved in *N,N*-dimethylacetamide (DMAc) by using the easy microwave heating method to synthesize CoNC. The mixture was filled in a microwave tube (5 mL), which was vacuumized and sealed in a glovebox. The microwave-assisted device was used by Biotage Initiator+ Microwave System, in which the microwave was heated at 200°C for 1.5 h using the power of the microwave irradiation was 90 W. The as-obtained sample was filtrated, washed with DMAc, THF and ethanol and finally dried at 50°C overnight. And FeNC was prepared using the similar procedures by replacing $\text{CoPc}(\text{NH}_2)_4$ with $\text{FePc}(\text{NH}_2)_4$. The isolated yields of CoNC and FeNC were 69% and 73%, respectively.

2.2. Instruments and parameters

Microwave-assisted device was used by Biotage Initiator+ Microwave System and the power of the microwave irradiation was 90 W. Ultraviolet-visible (UV-vis) spectra were procured in DMF at room temperature with a Shimadzu UV-2600 spectrophotometer. $^1\text{H NMR}$ spectra (liquid state) were recorded in Chloroform-*d* (CDCl_3) on AV-400 NMR spectrometer (Bruker), using TMS as an internal standard. X-ray photoelectron spectroscopy (XPS) analysis conducted with ESCALAB MK II X-ray instrument using an Al K α source was used to analyze the composition of the materials. Matrix-assisted laser desorption ionization time-of-flight mass (MALDI-TOF MS) spectra were recorded on Bruker Autoflex III. Element analysis was obtained on an Elementar vario EL cube instrument. Fluorescence spectra were measured on a PerkinElmer LS-55 Fluorescence Spectrometer using appropriate filters. Specific surface areas were calculated using the Brunauer-Emmett-Teller (BET) model via Quantachrome NOVA2200e nitrogen adsorption apparatus. Fourier transform infrared spectra (FTIR) measurements performed on a PerkinElmer Frontier spectrometer using KBr pellets technique with the scanning from 400 to 4000 cm^{-1} . The microstructures of the samples were studied by scanning electron microscopy (SEM Hitachi S-4800). Mechanical stress-strain measurements were obtained by microcomputer controlled single-arm electronic universal testing machine (WDW-01T). All the electrochemical measurements were performed on CS350 Electrochemical Workstation (Wuhan CorrTest Instruments Co., Ltd.).

2.3. Preparation of the electrodes

2.3.1. Preparation of the flexible MNCCs ($M = \text{Co}, \text{Fe}$) films

Firstly, MNC and CNTs with the appropriate amount were separately added into *N*-methylpyrrolidone (NMP) under the action of ultrasound. Next, the above two suspensions were mixed and further stirred for 12 h under the action of ultrasound. Then, the polyvinylidene fluoride microporous membrane ($0.22 \mu\text{m}$) was used to vacuum filtrate the homogeneous suspensions. As last, the as-obtained flexible films were dried at 50°C overnight under vacuum. For comparison, various MNCCs with different proportion by weight of MNC and MWCNT (1:1, 1:2, 1:3 and 1:5) were synthesized (named as MNCCs- x , $x = 1, 2, 3$ and 5). The pure CNT film was synthesized using the similar way without the addition of MNC.

2.3.2. Preparation of CoNC electrode

Since the CoNC powder cannot be directly fabricated for the supercapacitor electrode, the electrode was prepared by the following method: the as-prepared active materials CoNC, acetylene black and poly(vinylidene fluoride) (PVDF) binder were first mixed in NMP with 8:1:1 wt%. Then, the slurry was coated on a titanium form ($1.0 \text{ cm} \times 2.0 \text{ cm}$), which was vacuum dried at 70°C for 12 h.

2.4. Electrochemical measurements

The electrochemical properties of the as-prepared sample were tested on a three-electrode system. And 1 M H₂SO₄ solution was used as electrolytes, a platinum foil as the counter electrode, an Ag/AgCl electrode (saturated KCl solution) as the reference electrode and the CoNC electrode or the CoNCCs flexible electrode was used as a working electrode. The electrochemical test of the CoNCCs flexible electrode and the CoNC electrodes were carried out with potentials ranging from -0.15 to 1.45 V. The cyclic voltammetry (CV) curves were performed using different sweep speeds from 5 to 200 mV s⁻¹ and the galvanostatic charge-discharge (GCD) measurements were tested at different current densities. The specific capacitance was calculated according to the reported literature [42].

3. Results and discussion

The CoPc(NO₂)₄ is synthesized by a typical solid-state method. And CoPc(NH₂)₄ is reduced from CoPc(NO₂)₄ with Na₂S·9H₂O (Fig. S1). To confirm the successful synthesis of CoPc(NO₂)₄ and CoPc(NH₂)₄, UV-Vis absorption spectroscopy is carried out (Fig. S2). CoPc(NO₂)₄ shows two characteristic absorption bands of the B and Q bands. The Q-band is a double peak and appears at 615 nm and 661 nm, respectively. The shoulder peak around 615 nm is the weak vibrational absorption peak of the CoPc(NO₂)₄ dimer. CoPc(NH₂)₄ exhibits the double peaks of the Q-band appear at 648 nm and 706 nm, respectively. The shoulder peak around 648 nm is the weak vibrational absorption peak of the CoPc(NH₂)₄ dimer. Obviously, the Q band of CoPc(NH₂)₄ occurs the red shift resulted from the molecule conjugation effect [38]. In addition, the synthesis of CoPc(NO₂)₄ and CoPc(NH₂)₄ has been confirmed by Mass spectra (Fig. S3). And NBC is synthesized by tris(4-iodophenyl)amine and 4-formylphenylboronic acid (Fig. S4). ¹H NMR spectroscopy is used to demonstrate the successful synthesis of the obtained NBC (Fig. S5). Then the MNC is synthesized by the polycondensation reaction between CoPc(NH₂)₄ and NBC (Fig. 1), which is performed using the fast microwave heating way. Finally, the vacuum filtration way is used to prepare the flexible MNCCs films (Fig. 2). Interestingly, vacuum filtration method is a simple, safe, low-cost and mass produced. In addition, the easy vacuum filtration method is able to provide the films as the flexible electrodes. The flexible electrodes can be made into an integrated electrode by avoiding the use of binder in the preparation

process. Therefore, flexible electrodes show great advantages in bendability, ductility and long cycle life.

For purpose of determine the chemical components of samples, FT-IR tests are performed (Fig. 3a). The FT-IR spectrum of CoPc(NO₂)₄ displays vibrational absorption peaks of phthalocyanine skeleton at 1140, 1093, 760 and 726 cm⁻¹, which proves the formation of phthalocyanine macrocycles. The in-plane and out-plane vibrational absorption peaks of -NO₂ appear at 1521 and 1339 cm⁻¹, respectively. There is no characteristic absorption peak of C≡N appeared at about 2200 cm⁻¹, indicating the synthesis of CoPc(NO₂)₄ [39]. The FT-IR spectrum of CoPc(NH₂)₄ displays the N-H stretching peaks at 3344 and 3221 cm⁻¹ from the amino groups. And the phthalocyanine macrocycle shows the characteristic and vibration peaks at 1092 and 747 cm⁻¹, respectively. The bending vibration absorption peak of N-H in -NH₂ appears at 1609 cm⁻¹, while the characteristic absorption peak of -NO₂ disappears, suggesting the completely reduction from CoPc(NO₂)₄ to CoPc(NH₂)₄. Absorption band of NBC at 1701 cm⁻¹ is related with the stretching vibration of the carbonyl part of the aldehyde. FT-IR spectrum of CoNC shows peaks of residual -NH₂ groups within the scope of 3000–3500 cm⁻¹ [43], indicating some retained edge linkages. Moreover, the C=N stretching vibration contributed to the imine bond appear at 1609 cm⁻¹ [40,41]. At the meantime, the carbonyl part of CoNC is observably weakened, reflecting that CoNC is successfully synthesized. The fluorescence emission properties of the CoPc(NO₂)₄, CoPc(NH₂)₄ and CoNC polymers are investigated by fluorescence spectra in DMF (Fig. S6). Under excitation wavelength of 530 nm, CoPc(NO₂)₄, CoPc(NH₂)₄ and CoNC show the maximum emission spectral band at 637, 627 and 627 nm, indicating their fluorescence properties. To determine the oxidation state of Co, XPS measurement is tested. The high-resolution Co 2p XPS spectra of CoPc(NO₂)₄ show two pairs of 2p_{3/2}/2p_{1/2} doublets of Co²⁺ (796/780.2 eV) (Fig. S7). The specific surface area and porous structure of the CoNC are tested by nitrogen adsorption/desorption measurements. The Brunauer-Emmett-Teller (BET) surface area of CoNC is 14.727 m² g⁻¹ (Fig. S8). The pore size distribution of CoNC tested by BJH method (inset of Fig. S8) shows that the pore diameter is mainly distributed from 2 to 10 nm. Subsequently, the morphology of the sample is characterized using scanning electron microscope (SEM). The SEM image of CoNCCs shows that the granular CoNC is diffused on the surface of CNTs (Fig. S9a). In addition, the relevant energy dispersive X-ray spectroscopy (EDS) images confirm existence of Co, N and C

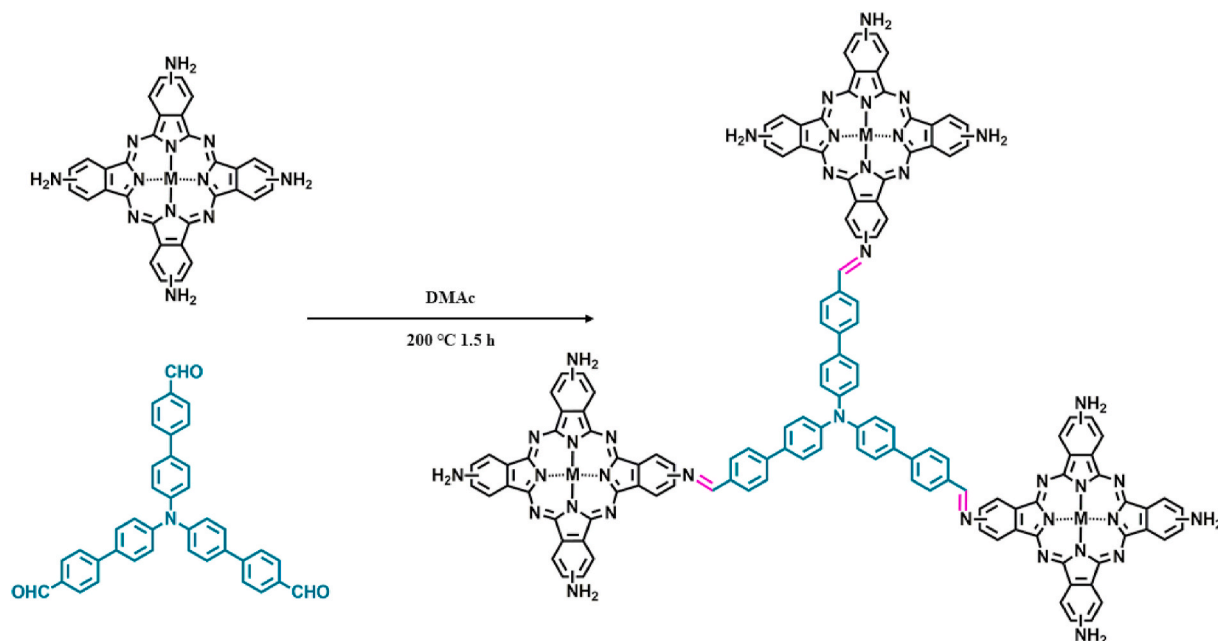


Fig. 1. Schematic synthetic process for the synthesis of MNC (M = Co, Fe).

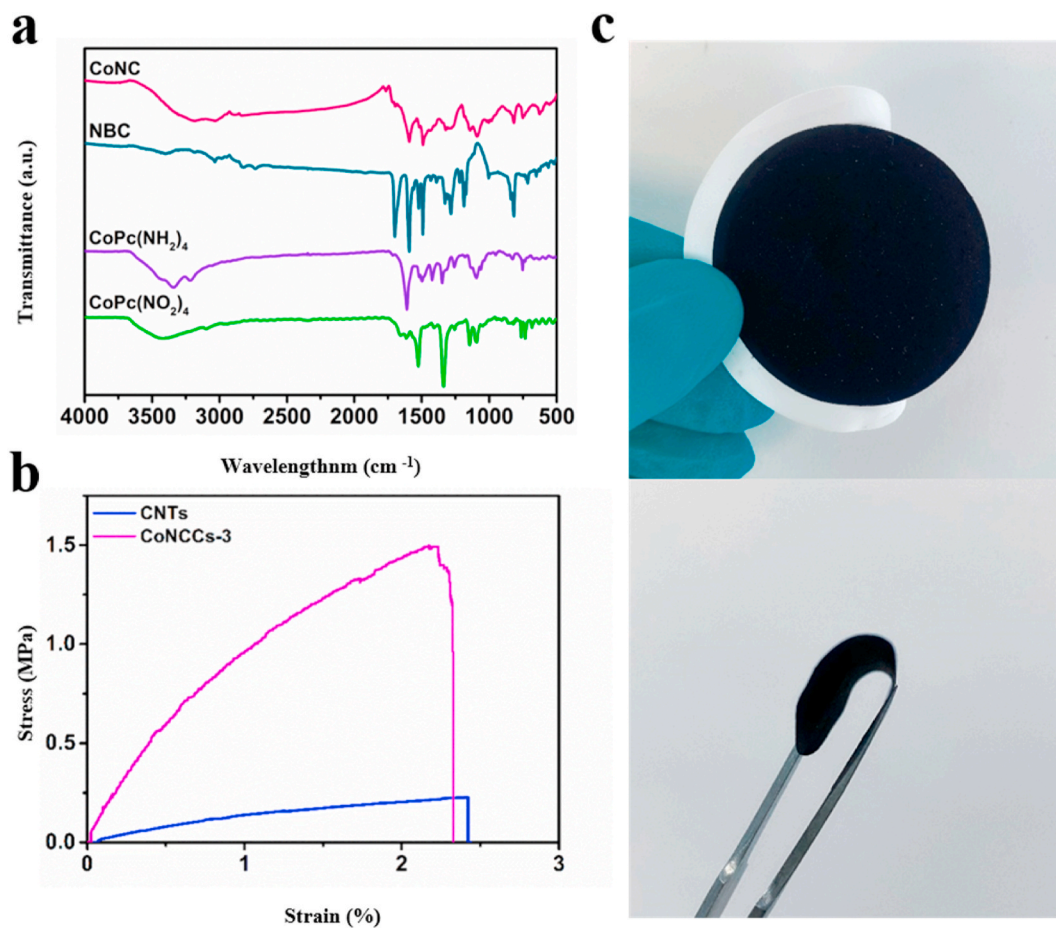


Fig. 3. (a) FT-IR spectra, (b) mechanical stress-strain curve, (c) digital photographs of flexible MNCCs (M = Co, Fe) electrode.

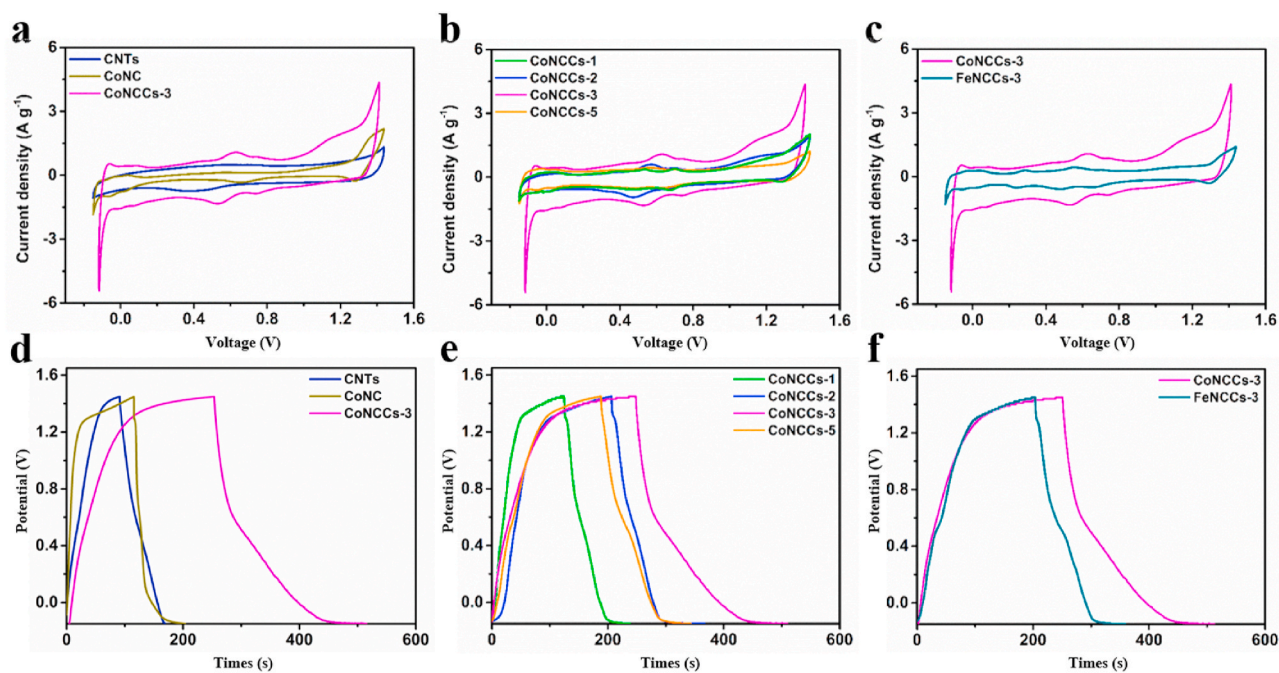


Fig. 4. Comparisons of the CV curves of (a) CNTs, CoNC and CoNCCs-3, (b) CoNCCs, (c) MNCCs-3 (M = Co, Fe) at a scan rate of 50 mV s⁻¹. Comparisons of the GCD curves of (d) CNTs, CoNC and CoNCCs-3, (e) CoNCCs, (f) MNCCs-3 (M = Co, Fe) at 1 A g⁻¹.

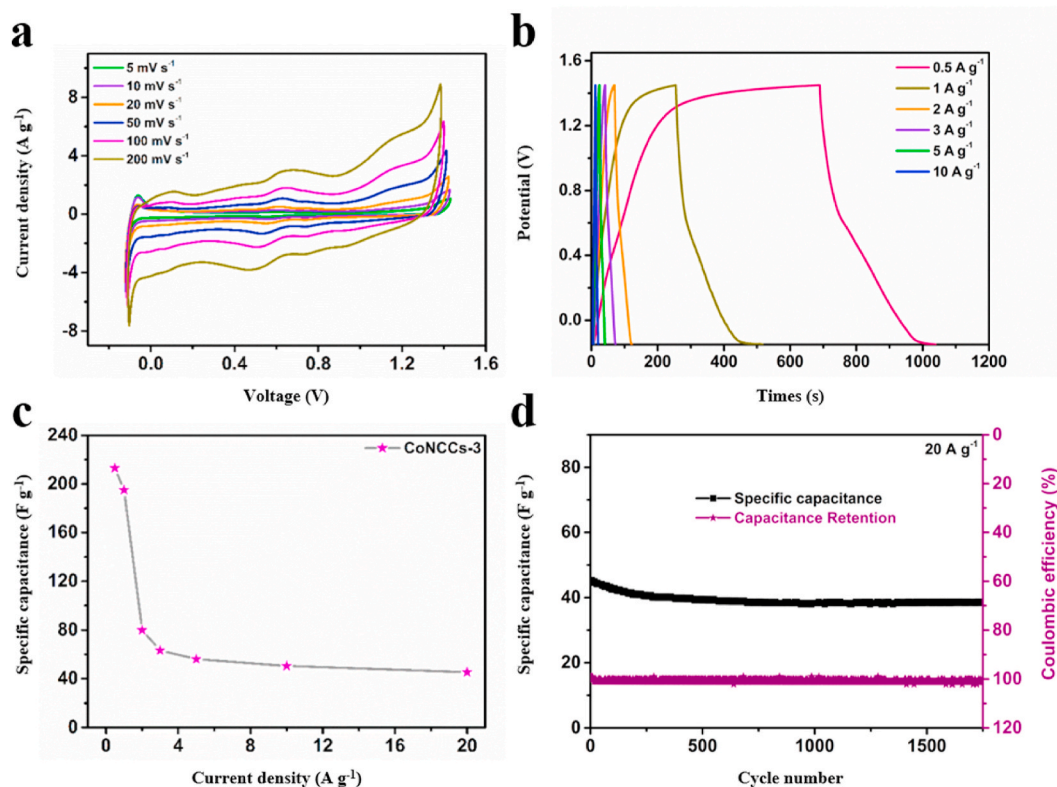


Fig. 5. (a) CV curves of CoNCCs-3 at different scan rates, (b) GCD curves of CoNCCs-3 obtained at different current densities, (c) specific capacitances of CoNCCs-3 at different current densities, (d) cycling performance and coulombic efficiency of CoNCCs-3 at 20 A g⁻¹.

(Fig. S10a). Pure CNTs show a CV curve with almost rectangular EDLC behavior (Fig. S10b). And FeNCCs-3 also shows a CV curve with pseudocapacitance characteristics (Fig. S10c). In addition to CoNCCs-3, CV curves of all the samples with different ratios between CoNC and CNTs (from 5 to 200 mV s⁻¹) are also studied (Figs. S11a–c). It can be noticed that CV curves exhibit typical pseudocapacitance characteristics. In addition, GCD curves of all the samples are performed at different current densities. CoNCCs-3 shows a larger plateau (Fig. 5b), which is similar to pure CoNC and FeNCCs-3, but different from pure CNTs (Fig. S12). The results are compliance with the CV curve. The relevant specific capacitance can be computed on the basis of GCD curves. CoNCCs-3 shows specific capacitances of 213.4, 195.3, 79.8, 63.3, 53.9, 49.5 and 45.4 F g⁻¹ at the current densities of 0.5, 1, 2, 3, 5, 10 and 20 A g⁻¹, respectively (Fig. 5c). By comparison, pure CoNC exhibits specific capacitances of 55, 18, 11, 7.6 and 6.9 F g⁻¹ at 1, 2, 3, 5 and 10 A g⁻¹, respectively (Fig. S12a). The pure CNTs show the specific capacitance of 49, 47.5, 41.3, 36.9 and 32.2 F g⁻¹ at 1, 2, 3, 5 and 10 A g⁻¹, respectively (Fig. S12b). In addition, FeNCCs-3 shows specific capacitances of 99, 60, 50.5, 42.5 and 35.7 F g⁻¹ at 1, 2, 3, 5 and 10 A g⁻¹, respectively (Fig. S12c). Except as CoNCCs-3, the GCD curves of samples with different ratios of CoNC and CNTs are also studied (Fig. S13). It can be found that all GCD curves correspond to the corresponding CV curves. CoNCCs-1 shows the specific capacitances of 52, 30, 24.7, 20.3 and 16.7 F g⁻¹ at 1, 2, 3, 5 and 10 A g⁻¹ (Fig. S13a). CoNCCs-2 shows the specific capacitance of 100, 55, 44, 36 and 33 F g⁻¹ at 1, 2, 3, 5 and 10 A g⁻¹ (Fig. S13b). And CoNCCs-5 shows specific capacitance of 97.5, 69.5, 62, 51 and 41 F g⁻¹ at 1, 2, 3, 5 and 10 A g⁻¹, respectively (Fig. S13c). Obviously, the optimal ratio and synergy of CoNC and CNTs make the composite material with a higher specific capacitance. Moreover, CoNCCs-3 shows good cycle stability with high specific capacitance retention rate of 85.3% after 1750 cycles even at the higher current density of 20 A g⁻¹ (Fig. 5d). Overall, the good electrochemical performance is resulted from the high pseudo-capacitance of CoNC and the

synergistic effect of the capacitance contribution and good electrical conductivity CNTs.

4. Conclusions

We show an effective strategy to construct the composite film composed of CMP with triphenylamine aldehyde linked to metal phthalocyanines (M = Co and Fe) and high-conductivity CNTs by combining the microwave method and the vacuum filtration strategy. Interestingly, the composite film shows fascinating flexible features as binder-free and free-standing electrode for SCs. The highly active CoNC with metallic characteristics can be composited with highly conductive CNTs through the π - π interaction between them without any covalent bonds. Thanks to the synergistic effect between the high pseudocapacitance of CoNC and the great conductivity of CNTs, flexible electrode of CoNCCs has a high specific capacitance of 213.4 F g⁻¹ at 0.5 A g⁻¹ and the good capacity retention rate of 85.3% after 1750 cycles at 20 A g⁻¹. The synergy and powerful functions of the conjugated microporous polymer connected with metal phthalocyanine and triphenylamine aldehyde (MNC) and highly conductive CNTs offer the probability of developing higher performance supercapacitors.

Credit authorship contribution statement

Lan Mei: Investigation, Data curation, Writing- Original draft. **Xu Cui:** Formal analysis, Conceptualization. **Juncheng Wei:** Investigation. **Qian Duan:** Funding acquisition, Project administration, Writing- Reviewing and Editing. **Yanhui Li:** Funding acquisition.

Declaration of competing interest

The authors declare that they have no known competing financial interests or personal relationships that could have appeared to influence

the work reported in this paper

Acknowledgments

The authors are grateful for financial support from Jilin Science & Technology Department (20190303069SF, 20150520025JH and 20180520166JH).

Appendix A. Supplementary data

Supplementary data to this article can be found online at <https://doi.org/10.1016/j.dyepig.2021.109299>.

References

- Miller JR, Simon P. Electrochemical capacitors for energy management. *Science* 2008;321:651–2.
- Li L, Lu F, Xue R, Ma BL, Li Q, Wu N, Liu H, Yao WQ, Guo H, Yang W. Ultrastable triazine-based covalent organic framework with an interlayer hydrogen bonding for supercapacitor applications. *ACS Appl Mater Interfaces* 2019;11:26355–63.
- Najib S, Erdem E. Current progress achieved in novel materials for supercapacitor electrodes: mini review. *Nanoscale Adv* 2019;1:2817–27.
- Wang F, Wu X, Yuan X, Liu Z, Zhang Y, Fu L, Zhu Y, Zhou Q, Wu Y, Huang W. Latest advances in supercapacitors: from new electrode materials to novel device designs. *Chem Soc Rev* 2017;46:6816–54.
- Khattak AM, Sin H, Ghazi ZA, He X, Liang B, Khan NA, Alanagh HR, Iqbal A, Li LS, Tang ZT. Controllable fabrication of redox-active conjugated microporous polymer on reduced graphene oxide for high performance faradaic energy storage. *J Mater Chem A* 2018;6:18827–32.
- Béguin F, Presser V, Balducci A, Frackowiak E. Carbons and electrolytes for advanced supercapacitors. *Adv Mater* 2014;26:2219–51.
- Simon P, Gogotsi Y. Materials for electrochemical capacitors. *Nat Mater* 2008;7:845–54.
- Manjunatha N, Imadadulla M, Lokesh KS, Reddy KR. Synthesis and electropolymerization of tetra-[β -(2-benzimidazole)] and tetra-[β -(2-(1-(4-aminophenyl)benzimidazole))] embedded cobalt phthalocyanine and their supercapacitance behaviour. *Dyes Pigments* 2018;153:213–24.
- Wang YG, Song YF, Xia YY. Electrochemical capacitors: mechanism, materials, systems, characterization and applications. *Chem Soc Rev* 2016;45:5925–50.
- Han Y, Zhang Q, Hu NT, Zhang X, Mai YY, Liu JQ, Hua XL, Wei H. Core-shell nanostructure of single-wall carbon nanotubes and covalent organic frameworks for supercapacitors. *Chin Chem Lett* 2017;28:2269–73.
- Wang Y, Shi ZQ, Huang Y, Ma YF, Wang CY, Chen MM, Chen YS. Supercapacitor devices based on graphene materials. *J Phys Chem C* 2009;113:13103–7.
- Son H, Yang MH, Mutyalak AK, Chang DW, Park JS. Superior electrocatalytic performance of polyisobutylene-substituted metallophthalocyanines supported on single-walled carbon nanotubes for an oxygen reduction reaction. *Dyes Pigments* 2019;162:662–70.
- Feng E, Ma GF, Peng H, Hua FT, Tang W, Lei Z, Tang W, Lei ZQ. Sponge integrated highly compressible all-solid state supercapacitor with superior performance. *New J Chem* 2017;41:13347–54.
- Khalid M, Varela H. A general potentiodynamic approach for red phosphorus and sulfur nanodot incorporation on reduced graphene oxide sheets: metal-free and binder-free electrodes for supercapacitor and hydrogen evolution activities. *J Mater Chem A* 2018;6:3141–50.
- Cao JY, Zhao Y, Xu YF, Zhang Y, Zhang B, Peng HS. Sticky-note supercapacitors. *J Mater Chem A* 2018;6:3355–60.
- Tabrizi AG, Arsalani N, Mohammadi A, Namazi H, Ghadimi LS, Ahadzadeh I. Facile synthesis of a MnFe₂O₄/rGO nanocomposite for an ultra-stable symmetric supercapacitor. *New J Chem* 2017;41:4974–84.
- Zhang HH, Zhang YN, Gu C, Ma YG. Electropolymerized conjugated microporous poly(zinc-porphyrin) films as potential electrode materials in supercapacitors. *Adv Energy Mater* 2015;5:1402175.
- Ahn H, Huang YC, Lin CW, Lee YH. Efficient defect healing of transition metal dichalcogenides by metallophthalocyanine. *ACS Appl Mater Interfaces* 2018;10:29145–52.
- Biyikoglu Z, Çakır V, Koca A, Kantekin H. Synthesis, electrochemical, in-situ spectroelectrochemical and in-situ electrochromic characterization of non-peripheral tetrasubstituted metal-free and metallophthalocyanines. *Dyes Pigments* 2011;89(1):49–55.
- Tang Q, Li L, Song Y, Liu Y, Li H, Xu W, Liu Y, Hu W, Zhu D. Photoswitches and phototransistors from organic single-crystalline sub-micro/nanometer ribbons. *Adv Mater* 2007;19:2624–8.
- Mu JB, Shao CL, Guo ZC, Zhang MY, Zhang ZY, Zhang P, et al. Solvothermal synthesis and electrochemical properties of 3D flower-like iron phthalocyanine hierarchical nanostructure. *Nanoscale* 2011;3:5126–31.
- Lekitima JN, Ozoemena KI, Jafta CJ, Kobayashi N, Song Y, Tong D, et al. High-performance aqueous asymmetric electrochemical capacitors based on graphene oxide/cobalt (II)-tetrapyrrolineporphyrin hybrids. *J Mater Chem A* 2013;1:2821–6.
- Nombona N, Nyokong T. The synthesis, cyclic voltammetry and spectroelectrochemical studies of Co(II) phthalocyanines tetra-substituted at the α and β positions with phenylthio groups. *Dyes Pigments* 2009;80(1):130–5.
- Colson JW, Woll AR, Mukherjee A, Levendoff MP, Spitzer EL, Shields VB, Spencer MG, Park J, Dichtel WR. Oriented 2D covalent organic framework thin films on single-layer graphene. *Science* 2011;332:228.
- Spitzer EL, Dichtel WR. Lewis acid-catalysed formation of two-dimensional phthalocyanine covalent organic frameworks. *Nat Chem* 2010;2:672–7.
- Mackintosh HJ, Budd PM, McKeown NB. Catalysis by microporous phthalocyanine and porphyrin network polymers. *J Mater Chem* 2008;18:573–8.
- Spitzer EL, Colson JW, Uribe-Romo FJ, Woll AR, Giovino MR, Saldívar A, Dichtel WR. Lattice expansion of highly oriented 2D phthalocyanine covalent organic framework films. *Angew Chem Int Ed* 2012;51:2623–7.
- Kang X, Han X, Yuan C, Cheng C, Liu Y, Cui Y. Reticular synthesis of the topology covalent organic frameworks. *J Am Chem Soc* 2020;142:16346–56.
- Agboola BO, Ozoemena KI. Synergistic enhancement of supercapacitance upon integration of nickel (II) octa [(3,5-bis(carboxylate)-phenoxy) phthalocyanine with SWCNT-phenylamine. *J Power Sources* 2010;195:3841–8.
- Gao J, Cheng C, Zhou X, Li Y, Xu X, Du X, et al. Synthesis of size controllable copper phthalocyanine nanofibers by simple solvent diffusion method and their electrochemical properties. *J Colloid Interface Sci* 2010;342:225–8.
- Nguyen HL, Gropp C, Ma YH, Zhu CH, Yagh OM. 3D covalent organic frameworks selectively crystallized through conformational design. *J Am Chem Soc* 2020;142:20335–9.
- Wu ZS, Zheng YJ, Zheng SH, Wang S, Sun CL, Parvez K, Ikeda T, Bao XH, Mullen K, Feng XL. Stacked-layer heterostructure films of 2D thiophene nanosheets and graphene for high-rate all-solid-state pseudocapacitors with enhanced volumetric capacitance. *Adv Mater* 2017;29:1602960.
- Zhuang X, Zhang F, Wu D, Feng X. Graphene coupled Schiff-base porous polymers: towards nitrogen-enriched porous carbon nanosheets with ultrahigh electrochemical capacity. *Adv Mater* 2014;26:3081–6.
- Wan Y, Liang Q, Cong TT, Wang XY, Tao YY, Sun MY, Li ZY, Xu S. Novel catalyst of zinc tetraamino-phthalocyanine supported by multi-walled carbon nanotubes with enhanced visible-light photocatalytic activity. *RSC Adv* 2015;5:66286–93.
- Pan X, Fan Z, Chen W, Ding Y, Luo H, Bao X. Enhanced ethanol production inside carbon-nanotube reactors containing catalytic particles. *Nat Mater* 2007;6:507–11.
- Zhang HB, Dong X, Lin GD, Liang XL, Li HY. Carbon nanotube-promoted Co-Cu catalyst for highly efficient synthesis of higher alcohols from syngas. *ChemComm* 2005:5094–6.
- Ding XS, Han BH. Metallophthalocyanine-based conjugated microporous polymers as highly efficient photosensitizers for singlet oxygen generation. *Angew Chem Int Ed* 2015;54:6536–9.
- Li Q, Shao Q, Wu Q, Duan Q, Li YH, Wang HG. In situ anchoring of metal nanoparticles in N-doped carbon framework derived from metallophthalocyanine-based conjugated microporous polymers towards efficient oxygen reduction reaction. *Catal Sci Technol* 2018;8:3572–9.
- Mei L, Cui X, Duan Q, Li YH, Lv XL, Wang HG. Metal phthalocyanine-linked conjugated microporous polymer hybridized with carbon nanotubes as a high-performance flexible electrode for supercapacitors. *Int J Hydrogen Energy* 2020;45:22950–8.
- Ding XS, Han BH. Copper phthalocyanine-based CMPs with various internal structures and functionalities. *ChemComm* 2015;51:12783–6.
- Zhao YC, Wang T, Zhang LM, Cui Y, Han BH. Facile approach to preparing microporous organic polymers through benzoin condensation. *ACS Appl Mater Interfaces* 2012;4:6974–80.
- Chidembo AT, Ozoemena KI, Agboola BO, Gupta V, Wildgoose GG, Compton RG. Nickel (II) tetra-aminophthalocyanine modified MWCNTs as potential nanocomposite materials for the development of supercapacitors. *Energy Environ Sci* 2010;3:228–36.
- Schwab MG, Fassbender B, Spiess HW, Thomas A, Feng XL, Müllen K. Catalyst-free preparation of melamine-based microporous polymer networks through Schiff base chemistry. *J Am Chem Soc* 2009;131:7216–7.
- Liang XM, Gao Y, Duan JL, Liu ZF, Fang SL, Baughman RH, Jiang L, Cheng QF. Enhancing the strength, toughness, and electrical conductivity of twist-spun carbon nanotube yarns by π bridging. *Carbon* 2019;150:268–74.
- Amin K, Meng QH, Ahmad A, Cheng M, Zhang M, Mao LJ, Lu K, Wei ZX. A carbonyl compound-based flexible cathode with superior rate performance and cyclic stability for flexible lithium-ion batteries. *Adv Mater* 2018;30:1703868.